First-principles study of He trapping in η-Fe_2C*

Bing-Ling He(赫丙玲)[1,†], Jin-Long Wang(王金龙)[1], Zhi-Xue Tian(田之雪)[2], Li-Juan Jiang(蒋利娟)[1], Wei Song(宋薇)[1], and Bin Wang(王斌)[1]

[1] *College of Physics and Electronic Engineering, Xinxiang University, Xinxiang* 453003, *China*
[2] *College of Physics and Information Engineering, Hebei Normal University, Shijiazhuang* 050024, *China*

(Received 2 June 2016; revised manuscript received 7 August 2016; published online 30 September 2016)

The distribution of He in η-Fe_2C has been studied by first-principles calculations. The formation energies of interstitial He and substitutional He (replacing Fe) are 3.76 eV and 3.49 eV, respectively, which are remarkably smaller than those in bcc Fe, indicating that He is more soluble in η-Fe_2C than in bcc Fe. The binding potencies of both a substitutional-interstitial He pair (1.28 eV) and a substitutional-substitutional He pair (0.76 eV) are significantly weaker than those in bcc Fe. The binding energy between the two He atoms in an interstitial–interstitial He pair (0.31 eV) is the same as that in bcc Fe, but the diffusion barrier of interstitial He (0.35 eV) is much larger than that in bcc Fe, suggesting that it is more difficult for the interstitial He atom to agglomerate in η-Fe_2C than in bcc Fe. Thus, self-trapping of He in η-Fe_2C is less powerful than that in bcc Fe. As a consequence, small and dense η-Fe_2C particles in ferritic steels might serve as scattered trapping centers for He, slow down He bubble growth at the initial stage, and make the steel more swelling resistant.

Keywords: He bubble, η-Fe_2C, ferritic steels, first-principles

PACS: 68.55.A–, 71.15.Mb, 71.15.Nc **DOI:** 10.1088/1674-1056/25/11/116801

1. Introduction

Reduced-activation ferritic/martensitic (RAFM) steels are one of the most important candidates for the first-wall structural materials in fusion reactors,[1] partly due to their low swelling rates.[2] However, in a fusion reactor the energetic He atoms enter the first-wall structural material, while at the same time large amounts of He are produced from transmutation reactions. Due to the strong self-trapping,[3] and strong binding to vacancies,[4] hydrogen,[5] grain boundaries,[6–8] and dislocations,[9] high concentration He will form He bubble and induce void swelling.[10,11] Thus these steels still suffer He-induced embrittlement.[12]

Great effort has been made to suppress He bubble formation to improve the mechanical properties of the materials, and some alloying additions appear to work this way. For example, an experiment has demonstrated that the segregated Cr at the He bubble surface in a Fe-9Cr% steel slows down the Brownian motion of a small He bubble.[13] Hao *et al.*, using first-principles density functional theory (DFT) calculations, revealed that the segregated Cr increases the charge density at the bubble/Fe interface which prevents further He atoms passing through, and thus slows down the growth of He bubbles.[14] DFT calculations also demonstrated that Au[15] and Ce[16] have a more pronounced effect than Cr. C is one of the elementary chemical elements in ferritic steels, whose effect on the He migration and agglomeration in bcc Fe have also been investigated.[17] It is found that C inhibits the formation of higher order clusters composed of He and vacancies, i.e., He_nV_m, and thus increases the amount of He at substitutional positions at room temperature.

Due to its low solubility in ferritic steels, the excess carbon will precipitate in the form of carbides in quenched steels.[18,19] In the very initial stage, the C atoms occupied the octahedral sites in bcc Fe.[20] When the C content exceeds the equilibrium solubility, the cementite, θ-Fe_3C, is formed. A further increase of the C content, the η-Fe_2C and χ-Fe_5C_2 will also appear. Recently, the structure and stabilization of the iron carbides, especially, θ-Fe_3C, η-Fe_2C, and χ-Fe_5C_2, have been investigated by first-principles studies.[21–26] Faraoun *et al.*[23] using DFT calculation pointed out that the energy needed for the formation of the χ-Fe_5C_2 is three times larger than that to form η-Fe_2C. Denisov *et al.* studied the influence of heat treatment on the interaction between hydrogen and RUSFER-EK-181 Russian ferritic–martensitic steel, using the method of thermodesorption mass spectrometry, and they found that after soaking of martensitic steels at low-temperature tempering, clusters of carbon atoms are observed and metastable carbides (Fe_2C) appear.[27] Despite this, η-Fe_2C is not stable at any temperature and has been scarcely investigated experimentally in the modified martensitic steel.[28] However, previous investigations have showed that it may be stabilized by impurity elements[22,29] and may be produced by the irradiation

*Project supported by the Research Key Project of Science and Technology of Education Bureau of Henan Province, China (Grant Nos. 14A140030, 15A140032, 15B150010, and 15A430037) and the Innovation Talents Program of Science and Technology of Institution of Higher Education of Henan Province, China (Grant No. 14HASTIT044).

†Corresponding author. E-mail: hbl626@126.com

© 2016 Chinese Physical Society and IOP Publishing Ltd

in extreme conditions in connection with realization of international projects ITER.[30] Furthermore, Mazumder *et al.*[31] examined He implantation of an F82H tempered martensitic steel at different temperatures, and suggested that the carbide precipitates prevent He bubbles formation by trapping the diffusing He at low temperature. Our previous studies have declared that θ-Fe_3C in ferritic steels might mitigate He bubble growth[32] just as dispersed oxide particles[33,34] and smaller grains do.[35] Thus, η-Fe_2C is one of the most frequently observed carbide-precipitate phases, its effect on He bubble growth in bcc iron is in urgent need to understand. Due to the lattice mismatch at the interface leaves abundant free volumes (low electron density region) which are strong traps for He, the carbide/Fe interface will be as crucial as, if not more than, the inside of the carbide particles. As a first step to tackle the η-Fe_2C effect on He accumulation, in this work, we focus on the properties of He inside the grain of a η-Fe_2C particle in micro-meter scale, which can be well represented by a bulk system. Our calculations demonstrate that He is more soluble in η-Fe_2C than in bcc Fe and the He self-trapping in η-Fe_2C is less powerful than that in bcc Fe, indicating that η-Fe_2C particles in ferritic steels will trap more He atoms and might slow down He bubble growth at the initial stage, which may make the steel more swelling resistant.

2. Computational details

2.1. Electronic structure calculations

Our spin-polarized first-principles calculations were performed by the Vienna *ab initio* simulation package (VASP).[36–38] The electron–ion interaction was described using the projector augmented wave (PAW) method.[39,40] The electron exchange and correlation were treated within the generalized gradient approximation (GGA), using the Perdew Burke Ernzerhof (PBE) functional.[41] The cutoff energy for the plane wave basis set was taken as 400 eV. The stopping criterion for ionic relaxations was convergence of the total energy to within 10^{-4} eV.

2.2. Model system and properties calculated

In the primitive cell of η-Fe_2C, there are four Fe_{4g} and two C_{2a} atoms. The optimized lattice parameters are $a = 4.71$ Å, $b = 4.28$ Å, and $c = 2.82$ Å, which are consistent with the experimental results.[42] The calculated magnetic moments on Fe and C atoms are $1.66\mu_B$ and $-0.14\mu_B$, respectively, which is in agreement with the previous previous theoretical values.[23]

A 2×2×3 supercell with the fixed cell axes based on the optimized lattice parameter was used to trap the He atom. The sketch map for He at different interstitial sites is shown in Fig. 1. The Brillouin-zone integration was performed within Monkhorst–Pack scheme[43] using a uniform (3×3×3) mesh. The volume and shape of the system with the He atom were fixed but all the internal freedoms were fully relaxed. The formation energy of He at an interstitial site is defined as the energy needed to put it into that position from the free gas state as

$$E_{\text{int}} = E(\text{He/carbide}) - E(\text{carbide}) - E(\text{He}), \quad (1)$$

where E(He/carbide) and E(carbide) are the total energies of the η-Fe_2C systems with and without a He atom at the interstitial site, respectively, and E(He) is the energy of a He atom in gas. Since the interaction of He in free gas is negligibly small, we here take E(He) as zero. The formation energy of a He atom substituting a Fe or C atom is

$$E_{\text{sub}} = E(\text{He/carbide}_{\text{vac}}) - E(\text{carbide}) + E(\text{atom}), \quad (2)$$

where $E(\text{He/carbide}_{\text{vac}})$ is the total energy of the supercell with a He atom at a Fe or a C vacancy, E(atom) is the energy of a Fe atom in the bulk Fe or the energy of a C atom embedded in the 4×4×4 bulk Fe. The calculated Fe or C vacancy formation energy follows: $E_{\text{vac}} = E(\text{carbide}_{\text{vac}}) - E(\text{carbide}) + E(\text{atom})$, in which $E(\text{carbide}_{\text{vac}})$ is the total energy of the supercell with a Fe or a C vacancy.

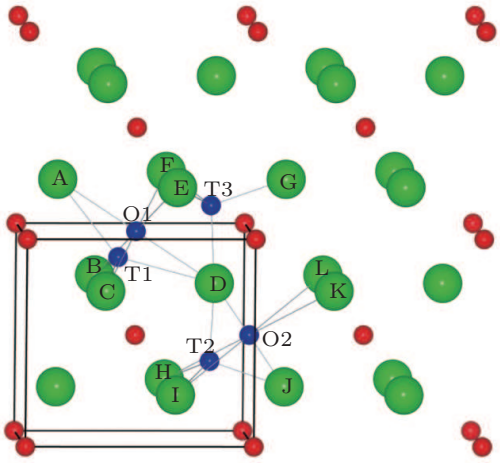


Fig. 1. (color online) The sketch map for He at different interstitial sites in η-Fe_2C. Green and red spheres represent the Fe and C atoms, respectively. The blue spheres denote different interstitial sites. Here, T1, T2, and T3 represent the tetrahedral interstices and O1 and O2 represent the octahedral interstices. The Fe atoms are distinguished by A, B, C, D, E, F, G, H, I, J, K, and L. The primitive cell of η-Fe_2C is enclosed by the black lines.

The binding energies between the two He atoms in an interstitial–interstitial (int–int) He pair, a substitutional–substitutional (sub–sub) He pair and a substitutional-interstitial (sub–int) He pair are defined as

$$\begin{aligned} E_{\text{int-int}} &= E_{\text{int}} - \{E(\text{He}_2/\text{carbide}) \\ &\quad - E(\text{He/carbide})\}, \quad (3) \\ E_{\text{sub-sub}} &= E_{\text{sub}} - \{E(\text{He}_2/\text{carbide}_{\text{vac2}}) \end{aligned}$$

$$-E(\mathrm{He/carbide_{vac}})\}, \quad (4)$$

$$E_{\mathrm{sub-int}} = E_{\mathrm{int}} - \{E(\mathrm{He_2/carbide_{vac}}) - E(\mathrm{He/carbide_{vac}})\}, \quad (5)$$

where $E(\mathrm{He_2/carbide})$ and $E(\mathrm{He_2/carbide_{vac2}})$ are the total energies of the systems with two interstitial He atoms and two substitutional He atoms, respectively, and $E(\mathrm{He_2/carbide_{vac}})$ is the total energy of the system with one interstitial He atom and one substitutional He atom. According to the definitions above, the binding energy of a He pair is the lowering of the total energy of the whole system when two He atoms are brought near from afar. We should note that positive formation energies correspond to endothermic processes for the He atom inserted at the interstitial or substitutional site, while positive binding energy of a He pair represents the attraction between the two He atoms.

In order to make a comparison, a 4×4×4 supercell of the bcc Fe was used to calculate the formation energy of the interstitial and substitutional He atoms, as well as the binding energy of a He pair.

3. Results and discussion

Due to its closed 1s shell, He can only interact repulsively with other elements under compression, thus He almost always prefers larger free volume, i.e., low electron density space. In the unit cell of η-Fe_2C, two octahedral (O1 and O2) and three tetrahedral interstices (T1, T2, and T3) have been investigated (Fig. 1). The O1 site is embraced by six Fe atoms "A", "B", "C", "D", "E", and "F" and the O2 site is also embraced by six Fe atoms "D", "H", "I", "J", "K", and "L". The two octahedral interstices have the same volume (9.5 $\mathrm{Å}^3$), 26% larger than that in bcc Fe. The T1 and T2 sites are inside the O1 and O2 octahedrons, respectively, while the T3 site is surrounded by four Fe atoms "D", "E", "F", and "G".

The formation energies of the He atoms at different interstices were calculated according to Eq. (1) and listed in Table 1. Interstitial He at T1 and T2 sites are not stable, and they both slide to the neighboring octahedral interstices after full optimization. The formation energy of the He atom at T3 site is 4.22 eV. Although the two octahedral interstices have the same volume, the formation energies of the He atoms at the two sites are very different. The octahedral interstice O2 is the most favorable site for He with the formation energy of 3.76 eV, while the structure with the He atom at O1 site has a much larger formation energy of 4.25 eV. In order to find the underlying reason for the discrepancy, we provided the initial and optimized structures with He at O1 and O2 sites and the charge densities of the octahedral planes in Fig. 2. The relevant structural parameters are given in Table 2. From Table 2 and Fig. 2, we can see that, for the initial structure of He at O1 site, the distances between the He atom and its surrounding Fe atoms are between 1.91 Å and 1.95 Å, while for the optimized structure, the corresponding distances are increased to 2.09 Å and 2.18 Å, respectively. For He at O2 site, the distances of He–D and He–J are increased to 1.78 Å from 1.29 Å, and the other four bond lengths are increased to 2.53 Å from 2.40 Å. The volume of the optimized O1 interstice with He is 12.7 $\mathrm{Å}^3$, while that of O2 is 14.4 $\mathrm{Å}^3$. Thus, much larger volume change for O2 interstice (4.9 $\mathrm{Å}^3$) than O1 interstice (3.2 $\mathrm{Å}^3$) may be responsible for the lower formation energy of He at O2 than at O1 site. Due to the great difference between the bond lengths of He and its surrounding Fe atoms in interstice O2, we provided the charge densities of two octahedral planes in Figs. 2(f) and 2(g). The charge density of the plane composed by Fe atoms "A", "C", "D", and "F" in O1 is shown in Fig. 2(e). It is found that the charge densities near the He atom at O2 site are much lower than those at O1 site, which is in accordance with the smaller formation energy for He at O2 than O1 site.

Table 1. The formation energies (in eV) of He at interstitial and substitutional sites in η-Fe_2C, as well as the formation energies of He at the tetrahedral interstice (T) and the substitutional site (Fe) in bcc Fe. For an explanation of He positions in η-Fe_2C, please see Fig. 1.

Interstitial He at				Substitutional He for		
bcc Fe	η-Fe_2C			bcc Fe	η-Fe_2C	
T	O1	O2	T3	Fe	Fe	C
4.61	4.25	3.76	4.22	4.38	3.49	5.09

We have also calculated the spin magnetic moments of the systems with He at O1 or O2 sites, as shown in Table 2. The induced magnetic moments on the He atoms are less than $0.03\mu_B$, and the magnetic moments on the C atoms have no change compared with the pure η-Fe_2C. By contrast, because He behaves as a bonding insulator leading to the d-orbital hybridization reduction of its neighboring Fe atoms from one another, all the spin magnetic moments on Fe atoms surrounding the He atom are increased.[32,44]

The formation energies for He substitution of a Fe and a C atoms were calculated according to Eq. (2), and the corresponding formation energies are 3.49 eV and 5.09 eV, respectively. The He atom at the substitutional Fe site is 0.27 eV more stable than that at the interstitial site and it is much smaller than that in bcc Fe (4.38 eV). The formation energy of substitutional He can be decomposed into two events, forming a vacancy and trapping an interstitial He atom into a vacancy. The Fe and C vacancy formation energies are 1.80 eV and 0.94 eV, respectively, and the attraction between an interstitial He atom and the Fe vacancy is 2.07 eV, which is a little smaller than that in bcc iron, 2.49 eV. Thus, the smaller formation energy of substitutional He in η-Fe_2C is due to the smaller formation energies of Fe vacancy and interstitial He.

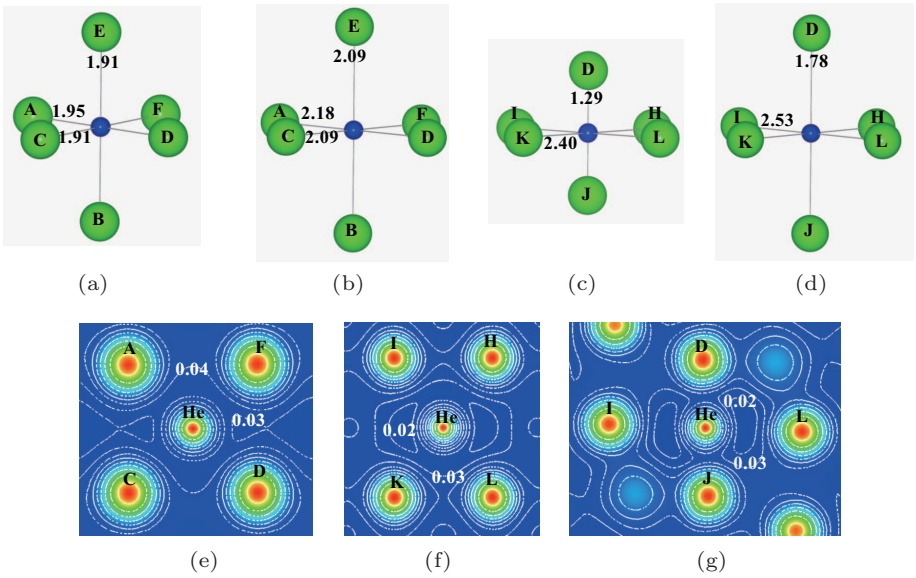


Fig. 2. (color online) The local configurations for He at O1 site before (a) and after (b) optimization, and at O2 site before (c) and after (d) optimization. Panel (e) is the calculated total valence charge densities for the octahedral planes of O1, and panels (f) and (g) are for O2. Lines start from 0.01 e/a.u.^{3}, and increase successively by a factor of $10^{1/5}$.

Table 2. Spin magnetic moments (M) of Fe atoms neighboring the He atom implanted into η-Fe_2C and their distances (d_{O1-X} and d_{O2-X}) away from the He atom, which is located at interstitial site O1 or O2, before and after relaxation. For an explanation of lattice sites A–L, and the interstitial sites O1 and O2, see Fig. 1.

Site X	d_{O1-X}/Å		M/μ_B	Site X	d_{O2-X}/Å		M/μ_B
	No He	He@O1	He@O1		No He	He@O2	He@O2
A	1.95	2.18	1.82	D	1.29	1.78	1.84
B	1.91	2.09	1.71	H	2.40	2.53	1.76
C	1.91	2.09	1.71	I	2.40	2.53	1.76
D	1.95	2.18	1.82	J	1.29	1.78	1.84
E	1.91	2.09	1.71	K	2.40	2.53	1.76
F	1.91	2.09	1.71	L	2.40	2.53	1.76

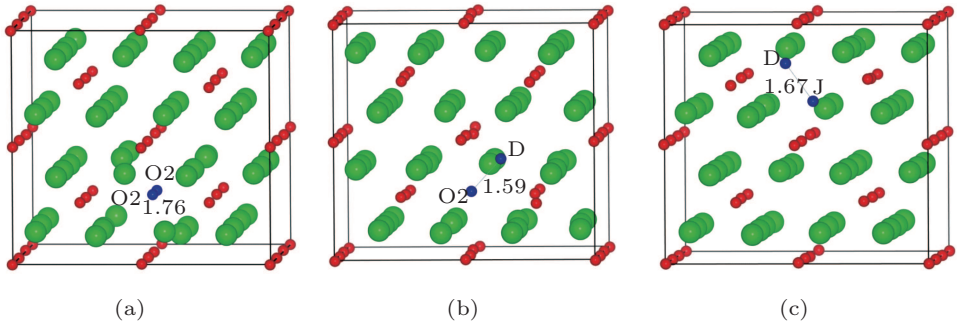


Fig. 3. (color online) The optimized structures of He pairs with two interstitial He atoms (a), one He atom at the substitutional site and the other at the interstitial site (b) and two He atoms at the substitutional sites (c).

The formation of a He pair is the initial stage of He bubble growth. Our objective in the present work is to elucidate the accumulation of He at the very initial state, i.e., pairing of He, and compare its easiness with that in the bcc Fe matrix. The binding energies between the two He atoms of a He pair can be considered as the reduction of the total energy when the two favorable interstitial (or substitutional), as well as one substitutional and one interstitial He atoms come nearby. The calculated binding energies are listed in Table 3, according to Eqs. (3)–(5). We have investigated four int–int, five sub–sub and three sub–int He pairs. The most stable int–int He pair is shown in Fig. 3(a). The two He atoms are at the neighboring O2 sites with the binding energy of 0.31 eV, as large as that in bcc Fe. The calculated diffusion barrier of interstitial He is 0.35 eV, much larger than that in bcc Fe (0.06 eV), indicating that it is more difficult for two interstitial He atoms to form a He pair in η-Fe_2C than in bcc Fe. The most stable sub–sub He pair is formed by two He atoms replacing two Fe atoms "D" and "J" with a binding energy of 0.76 eV, which is much smaller than that in bcc Fe (1.18 eV), shown in Fig. 3(c). The

formation energies for the three investigated sub–int He pairs are the same, 1.28 eV. All of them are much smaller than the binding energy of the sub–int He pair in bcc Fe (1.86 eV). Figure 3(b) is the optimized structure of the sub–int He pair with one He atom replacing Fe atom "D" and one He atom at O2 site. From Fig. 3, we can see that the distances between the two He atoms in the int–int, sub–sub, and sub–int He pairs are 1.76 Å, 1.67 Å, and 1.59 Å, respectively, indicating stronger binding corresponding to smaller distance between the two He atoms in a He pair.

Table 3. The binding energies (in eV) of int–int, sub–int, and sub–sub He pairs in η-Fe_2C. The values in the parentheses are the binding energies of the most stable int–int, sub–int, and sub–sub He pairs in bcc Fe. For an explanation of He positions, please see Fig. 1.

Int-int		Sub-int		Sub-sub	
He@	$E_{\text{int-int}}$	He@	$E_{\text{sub-int}}$	He@	$E_{\text{sub-sub}}$
O2 and O2	0.31(0.31)	D and O2	1.28(1.86)	D and B	0.03
O2 and O1	–0.07	D and O1	1.28	D and H	0.1
O2 and T2	–0.64	D and T3	1.28	D and J	0.76(1.18)
O2 and T3	–0.11			B and C	–0.02
				B and H	–0.06

From the numerical results above, we know that the formation energies of substitutional He are smaller than those of the interstitial He in both η-Fe_2C and bcc Fe. The occupation probabilities of He at the interstitial and substitutional sites in η-Fe_2C and bcc Fe could be estimated by McLean's equation as

$$C = \frac{C_{\text{bulk}} \exp(-\Delta E/k_{\text{B}}T)}{1 + C_{\text{bulk}} \exp(-\Delta E/k_{\text{B}}T)},$$

where ΔE is the energy difference between the formation energies for He at the two compared sites, i.e., the formation energy for He at the more stable site minus that of the less stable site, C_{bulk} is the He concentration and k_{B} is the Boltzmann's constant. In fusion reactors, the production of He in ferritic/martensitic steels due to the fusion neutrons amounts to 200–500 appm (atomic parts per million) per year,[45] thus we chose 200 appm and 500 appm as the He concentrations in Fig. 4. Furthermore, due to that the Curie temperature of η-Fe_2C is around 653 K,[46] we chose 600 K as the high temperature. From our calculations, we know that the energy differences between the formation energies of He at the interstitial and substitutional sites are -0.27 eV and -0.23 eV in η-Fe_2C and in bcc Fe, respectively. From Fig. 4, we can see that He mainly occupies the substitutional site at 300 K, and will occupy either the interstitial or the substitutional sites at 600 K both in η-Fe_2C and bcc Fe. The energy difference between the formation energies of the interstitial He in η-Fe_2C and bcc Fe is -0.85 eV, and that of the substitutional He is -0.89 eV. Thus, He mainly preferred to stay in η-Fe_2C both at low and high temperature, compared with bcc Fe.

From the calculations of the He pairs, we know that the binding energies between the two He atoms of a sub–sub He pair (0.76 eV) and a sub–int He pair (1.28 eV) are much smaller than those in bcc Fe (1.18 eV and 1.86 eV). In order to find the reason for this, we provided the charge densities of He at the substitutional site, a sub–int He pair and a sub–sub He pair in η-Fe_2C in Fig. 5. From Fig. 5(a), we can see that there is a high charge density area near He. This is because in η-Fe_2C, one C atom bonded with two Fe atoms and when one Fe atom substituted by the He atom, one C–Fe bond broke, which will create higher electron density area near the C atom. This may explain why the attraction between an interstitial He atom and the Fe vacancy in η-Fe_2C (2.07 eV) is much smaller (0.42 eV) than that in bcc Fe (2.49 eV). From Figs. 5(b) and 5(c), we can see that there are one and two C atoms near the sub–int He pair and the sub–sub He pair, respectively, due to one C–Fe bond and two C–Fe bonds breaking. Furthermore, the charge densities for the transition state of He diffusion in Fig. 5(d) shows that the densities of the area near the C–Fe bonds are much higher than those of the other areas encircling the inserted He atoms. Thus, we attribute the less powerful self-trapping of He in η-Fe_2C than in bcc Fe to the repulsive interaction between He and C. Our results are in good agreement with the previous research, in which, it is suggested that C inhibits the formation of higher order clusters composed of He and vacancies, i.e., He_nV_m, and thus increases the number of He at substitutional positions at room temperature.[17]

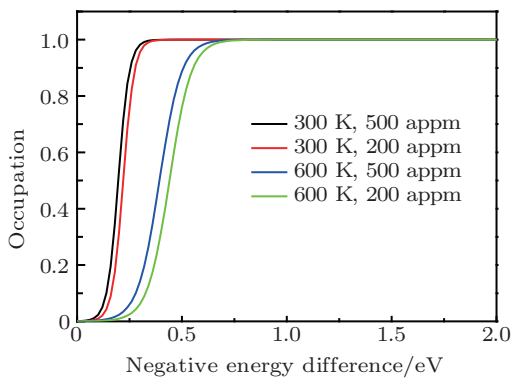


Fig. 4. (color online) The calculated occupation probability of He as a function of the energy difference at different temperatures and bulk concentrations based on the McLean's equation.

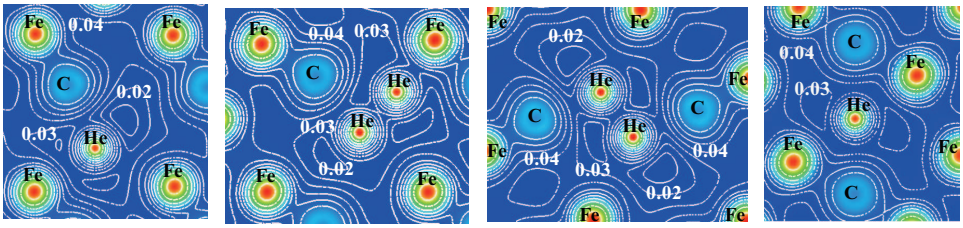


Fig. 5. (color online) The calculated total valence charge densities for (a) the (001) plane with He at the substitutional site, (b) the plane with a sub–int He pair, (c) the plane with a sub–sub He pair and (d) the (001) plane of the transition state of He diffusion. Lines start from $0.01e$/a.u.^{3}, and increase successively by a factor of $10^{1/5}$.

4. Conclusions

In summary, we have systematically investigated the stability of He inside the η-Fe_2C bulk by first-principles calculations based on the density functional theory. The formation energies of the He atoms at the substitutional and interstitial sites in η-Fe_2C are 3.49 eV and 3.76 eV, respectively, which is much smaller than those in bcc Fe. The binding energies between two interstitial He atoms is as large as that in bcc Fe, 0.31 eV. However, the diffusion barrier of the interstitial He is 0.35 eV, which is much larger than that in bcc Fe. Furthermore, the binding potencies between two substitutional He atoms and one substitutional and one interstitial He atoms (0.76 eV and 1.28 eV) are much weaker than those in bcc Fe. The larger solubility of a He atom and weaker binding potency between two He atoms in η-Fe_2C than in bcc Fe might may make the small and dense η-Fe_2C particles in ferritic steels serve as scattered trapping centers for He and mitigate He bubble growth at the initial stage. We hope that this study will promote further experimental and theoretical efforts to design more swelling resistant steels taking advantage of carbides.

Acknowledgment

Bing-ling He is grateful to her advisor Wen-Tong Geng for his guidance in carrying out this research.

References

[1] Huang Q, Baluc N, Dai Y, Jitsukawa S, Kimura A, Konys J, Kurtz R J, Lindau R, Muroga T, Odette G R, Raj B, Stoller R E, Tan L, Tanigawa H, Tavassoli A F, Yamamoto T, Wan F and Wu Y 2013 *J. Nucl. Mater.* **442** S2
[2] Andreani R, Diegele E, Laesser R and van der Schaaf B 2004 *J. Nucl. Mater.* **329–333** (Part A) 20
[3] Wilson W, Bisson C and Baskes M 1981 *Phys. Rev. B* **24** 5616
[4] Seletskaia T, Osetsky Y, Stoller R E and Stocks G M 2005 *Phys. Rev. Lett.* **94** 046403
[5] Jiang B, Wan F R and Geng W T 2010 *Phys. Rev. B* **81** 134112
[6] Kurtz R J and Heinisch H L 2004 *J. Nucl. Mater.* **329–333** (Part B) 1199
[7] Smith R W, Geng W T, Geller C B, Wu R and Freeman A J 2000 *Scripta Mater.* **43** 957
[8] Tian Z X, Xiao W, Wan F R and Geng W T 2010 *J. Nucl. Mater.* **407** 200
[9] Berg F, Heugten W, Caspers L, Veen A and De Hosson J T M 1977 *Solid State Commun.* **24** 193
[10] Donnelly S E and Evans J H 1991 *Fundamental Aspects of Inert Gases in Solids*, (Plenum, New York) pp. 3–16
[11] Ishizaki T, Xu Q, Yoshiie T, Nagata S and Troev T 2002 *J. Nucl. Mater.* **307–311** (Part 2) 961
[12] Baluc N, Schäublin R, Spätig P and Victoria M 2004 *Nucl. Fusion* **44** 56
[13] Ono K, Arakawa K and Hojou K J 2002 *Nucl. Mater.* **307–311** Part 2 1507
[14] Hao W and Geng W 2012 *J. Phys.: Condens. Matter* **24** 095009
[15] Hao W and Geng W T 2011 *Nucl. Instrum. Methods Phys. Res., Sect. B* **269** 1428
[16] Hao W and Geng W T 2012 *Nucl. Instrum. Methods Phys. Res., Sect. B* **280** 22
[17] Ortiz C J, Caturla M J, Fu C C and Willaime F 2009 *Phys. Rev. B* **80** 134109
[18] Christian J W 2002 *The Theory of Transformations in Metals and Alloys (Part I+ II)* (Access Online via Elsevier) pp. 718–785
[19] Hofer L J E and Cohn E M 1951 *Nature* **167** 977
[20] Counts W A, Wolverton C and Gibala R 2010 *Acta Mater.* **58** 4730
[21] Fang C M, van Huis M A and Zandbergen H W 2010 *Scripta Mater.* **63** 418
[22] Ande C and Sluiter M F 2012 *Metall. Mater. Trans. A* **43** 4436
[23] Faraoun H I, Zhang Y D, Esling C and Aourag H 2006 *J. Appl. Phys.* **99** 093508
[24] Lv Z Q, Sun S H, Jiang P, Wang B Z and Fu W T 2008 *Comput. Mater. Sci.* **42** 692
[25] Fang C M, van Huis M A, Jansen J and Zandbergen H W 2011 *Phys. Rev. B* **84** 094102
[26] Bao L L, Huo C F, Deng C M and Li Y W 2009 *J. Fuel Chem. Technol.* **37** 104
[27] Denisov E, Kompaniets T N, Murzinova M A and Yukhimchuk A A 2013 *Tech. Phys.* **58** 814
[28] Coppola R, Dewhurst C D, Lindau R, May R P, Möslang A and Valli M 2004 *Physica B: Condens. Matter* **345** 225
[29] Naraghi R, Selleby M and Ågren J 2014 *Calphad* **46** 148
[30] Demina E V, Dubrovsky A V, Gribkov V A, Maslyaev S A, Pimenov V N, Sasinovskaya I P, Miklaszewski R and Scholz M 2009 *International Topical Meeting on Nuclear Research Applications and Utilization of Accelerators,* 2009, *IAEA, Vienna*
[31] Mazumdera B, Bannisterb M E, Meyerb F W, Millera M K, Parishc C M and Edmondson P D 2015 *Nucl. Mater. Energy* **1** 8
[32] He B L, Ping D H and Geng W T 2014 *J. Nucl. Mater.* **444** 368
[33] Hsiung L L, Fluss M J, Tumey S J, Choi B W, Serruys Y, Willaime F and Kimura A 2010 *Phys. Rev. B* **82** 184103
[34] Erhart P 2012 *J. Appl. Phys.* **111** 113502
[35] Yu K Y, Liu Y, Sun C, Wang H, Shao L, Fu E G and Zhang X 2012 *J. Nucl. Mater.* **425** 140
[36] Kresse G and Hafner J 1993 *Phys. Rev. B* **47** 558
[37] Kresse G and Furthmüller J 1996 *Comput. Mater. Sci.* **6** 15
[38] Kresse G and Furthmüller J 1996 *Phys. Rev. B* **54** 11169
[39] Blöchl P E 1994 *Phys. Rev. B* **50** 17953
[40] Kresse G and Joubert D 1999 *Phys. Rev. B* **59** 1758
[41] Perdew J P, Burke K and Ernzerhof M 1996 *Phys. Rev. Lett.* **77** 3865
[42] Hirotsu Y and Nagakura S 1972 *Acta Metall.* **20** 645
[43] Monkhorst H J and Pack J D 1976 *Phys. Rev. B* **13** 5188
[44] Yan J X, Tian Z X, Xiao W and Geng W T 2011 *J. Appl. Phys.* **110** 013508
[45] Schäublin R, Henry J and Dai Y 2008 *Comptes Rendus Physique* **9** 389
[46] Cohn E M and Hofer L J E 1953 *J. Chem. Phys.* **21** 354